Few-Layer MoS_2 with High Broadband Photogain and Fast Optical Switching for Use in Harsh Environments

Dung-Sheng Tsai,[†] Keng-Ku Liu,[‡] Der-Hsien Lien,[†] Meng-Lin Tsai,[†] Chen-Fang Kang,[†] Chin-An Lin,[†] Lain-Jong Li,[‡,§] and Jr-Hau He[†,*]

[†]Graduate Institute of Photonics and Optoelectronics, and Department of Electrical Engineering, National Taiwan University, Taipei, Taiwan, [‡]Institute of Atomic and Molecular Sciences, Academia Sinica, Taipei, Taiwan, and [§]Department of Photonics, National Chiao Tung University, Hsinchu, Taiwan

ABSTRACT Few-layered MoS_2 as Schottky metal—semiconductor—metal photodetectors (MSM PDs) for use in harsh environments makes its debut as two-dimensional (2D) optoelectronics with high broadband gain (up to 13.3), high detectivity (up to $\sim 10^{10}$ cm $Hz^{1/2}$/W), fast photoresponse (rise time of $\sim$70 μs and fall time of $\sim$110 μs), and high thermal stability (at a working temperature of up to 200 °C). Ultrahigh responsivity (0.57 A/W) of few-layer MoS_2 at 532 nm is due to the high optical absorption ($\sim$10% despite being less than 2 nm in thickness) and a high photogain, which sets up a new record that was not achievable in 2D nanomaterials previously. This study opens avenues to develop 2D nanomaterial-based optoelectronics for harsh environments in imaging techniques and light-wave communications as well as in future memory storage and optoelectronic circuits.

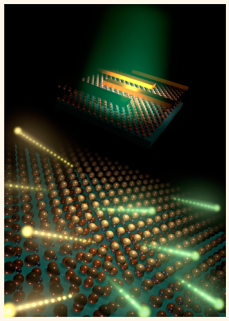

KEYWORDS: graphene · MoS_2 · photodetector · high-temperature detection · harsh environment

2D nanomaterials hold a promising future in next-generation electronics and photonics, benefiting from their unique planar advantages, such as the existence of quantum confinements and the absence of interlayer interactions, and thus allow us to achieve smaller, more flexible, and more efficient nanodevices.[1−5] Graphene, a 2D nanomaterial with rich physical phenomena, has been the most attractive target in the past few years.[6]

Nanomaterials are gaining intense interest in photodetection due to pronounced surface effects *via* very large surface-to-volume ratios and Debye lengths comparable to their feature size for potential applications in optoelectronics.[7−12] Until now, various 1D nanostructures have already displayed superior photosensitivity, and the related mechanism has been investigated over the years.[8−12] Among a variety of 2D nanomaterials, graphene produces an ultrafast photoresponse from ultraviolet (UV) to terahertz ranges due to the presence of an internal field formed near the interfaces of metal electrodes and the ability to absorb $\sim$2% of incident light over a broad wavelength range.[13,14] Although the ultrafast photodetection of 2D nanomaterials using pristine graphene is achieved, the responsivity of the pristin graphene photodetector (PD) is still unsatisfactory (1×10^{-3} A/W) mainly due to its zero band gap and short photocarrier lifetime, thus hindering practical applications of 2D nanomaterials in optoelectronics.[13−16] Consequently, the rapid development of graphene-based PDs is focused on the enhancement of the absorption of light by employing new materials or physical concepts.[17−20] For example, by combining graphene with plasmonic nanostructures, nanoparticles, or microcavity structures, the near-field enhancement or the increase of optical field absorption can significantly increase the responsivity of graphene-based PDs to $\sim$11, $\sim$6, and 21 mA/W, respectivly.[18−20] However, the responsivity is still limited due to the absence of photogain, *i.e.*, the ability to provide multiple electrical carriers per single incident photon. Until recently, Konstantatos *et al.* reported that the responsivity of hybrid graphene—quantum dot PDs is as high as 10^7 A/W due to the generation of photogain by using the

* Address correspondence to jhhe@cc.ee.ntu.edu.tw.

Received for review November 15, 2012 and accepted April 16, 2013.

Published online April 16, 2013
10.1021/nn305301b

© 2013 American Chemical Society

photogating effect, which is not achievable for pristine graphene.[17]

Atomic layered molybdenum disulfide (MoS_2), a newly emerging 2D nanomaterial with a direct and finite band gap, may provide a possible solution to surpass the shortages belonging to graphene.[21−25] Recently, gigantic photoluminescence (PL) enhancement of monolayer MoS_2 has been observed experimentally and theoretically (4-fold higher than its bulk counterpart).[24] This is due to a quantum confinement effect that expands the band gap from 1.2 eV (bulk) to 1.9 eV (monolayer) with a transition from "indirect band gap" to "direct band gap".[21−25] This strong PL of ultrathin MoS_2 implies possible applications in optoelectronics, such as PDs, biomedical markers, and sensors.[25] Very recently, as compared to that obtained from pristine graphene ($\sim 1 \times 10^{-3}$ A/W),[13,14] the high photoresponsivity (7.5×10^{-3} A/W) from MoS_2 phototransistors has been obtained due to direct band gap absorption.[26]

The capability of high-temperature operation would offer great advantages for future smart sensors working under harsh environmental conditions. Some group III−V and IV materials, especially diamond, SiC, and AlN, can fulfill the demands for high-temperature electronics and optoelectronics, exceeding the capabilities of Si devices.[27−29] For example, for high-temperature photodetection, SiC metal−semiconductor−metal (MSM) PDs have been demonstrated to work at 350 °C.[28,30] Although those PDs can be operated at a high temperature, all of them are wide-band-gap materials and thus capable of limited detection in only UV/deep UV regions rather than broadband photodetection.[27]

In this study, we report few-layer MoS_2 Schottky PDs with back-to-back MSM geometry, capable of broadband photodetection from visible to UV regions with working temperatures up to 200 °C for use in harsh environments. Until few-layer MoS_2 was demonstrated here, the broadband responsivity feature was not previously achievable for harsh environment use since all of the photodetection materials for harsh environments are wide-band-gap semiconductors. As a new record, the very high responsivity of 0.57 A/W and detectivity (over $\sim 10^{10}$ cm $Hz^{1/2}$/W) are due to high optical absorption of ~10% (very high absorption coefficient of up to 7.5×10^5 cm^{-1}) of the few-layer MoS_2 and a high photogain of ~13.3. In addition, temporal measurements reveal fast response times (~70 μs) and recovery times (~110 μs). The excellent optical properties of few-layer MoS_2 promise a new generation of fast, broadband PDs based on 2D nanomaterials for applications in harsh environments, such as sensing, imaging, and intrachip optical interconnects at high temperatures.

RESULTS AND DISCUSSION

Syntheses of high-quality few-layer MoS_2 by chemical vapor deposition have been reported recently.[31,32]

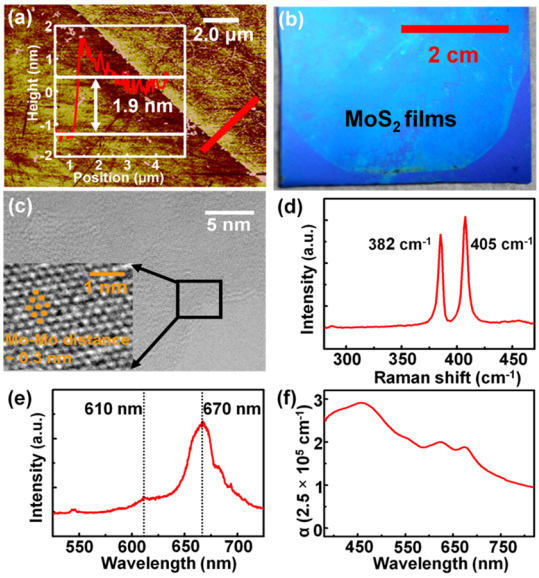

Figure 1. (a) AFM image and (b) photograph of the few-layer MoS_2 on a SiO_2/Si substrate. The inset shows the cross-sectional profile along the red line indicated in the AFM image in (a). (c) HRTEM image for the few-layer MoS_2. The inset shows an enlarged HRTEM image of the marked area in (c). (d) Raman spectrum, (e) PL, and (f) optical absorption spectrum of few-layer MoS_2 under ambient conditions at room temperature. Raman and PL measurements were performed in a confocal spectrometer using a 473 nm excitation laser.

Here, large-area and highly crystalline MoS_2 layers were prepared by a two-step thermolysis process (see Methods).[23] A line scan of atomic force microscopy (AFM) in Figure 1a reveals the edge of the thin MoS_2 layers with a distinct step of ~1.9 nm, corresponding to three MoS_2 layers (thickness of each layer: ~0.65 nm).[23] A photograph of few-layer MoS_2 is shown in Figure 1b. The high-resolution transmission electron microscopy (HRTEM) image in Figure 1c, showing periodic Mo atoms (with a distance of ~0.3 nm) arranging in hexagonal symmetry, confirms the crystallinity of the MoS_2 layers. The two Raman peaks in Figure 1d, *i.e.*, E^1_{2g} at 382 cm^{-1} and A_{1g} at 405 cm^{-1}, represent the characteristic active modes of MoS_2, where E^1_{2g} indicates the planar vibration and A_{1g} indicates the vibration of sulfides in the out-of-plane direction.[23,24] Moreover, the uniformity of few-layer MoS_2 can be characterized by Raman spectroscopy and optical microscopy. The energy difference (ΔE) between two Raman peaks (*i.e.*, 382 and 405 cm^{-1}) can be used to identify the number of MoS_2 layers. The calculated ΔE value is ~23 cm^{-1}, corresponding to trilayer MoS_2 films.[23] Few-layer MoS_2 in an insulating substrate grown by a two-step thermolysis process is uniform and continuous, based on the photograph shown in Figure 1b. The optimized process used here is able to produce very homogeneous MoS_2 trilayers across the whole sample. In general, the more diluted precursor solution and faster dip-coating result in a thinner MoS_2 layer. Here, we aim at large-area and superior-quality

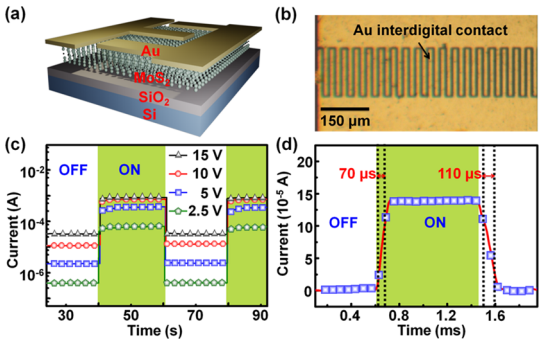

Figure 2. (a) Schematic and (b) optical microscopic top-view image of the few-layer MoS_2 MSM PDs. (c) Photocurrent as a function of time in the dark and under 532 nm laser illumination with a light intensity (I_{light}) of 2.0×10^4 W/m^2. (d) High-resolution time response of MoS_2 PDs measured at 5 V bias with $I_{light} = 2.0 \times 10^4$ W/m^2.

trilayer MoS_2 for PD applications. More details about the two-step thermolysis process can be found elsewhere.[23]

It has been known that direct band gap (at around 610 and 670 nm) and indirect band gap (from 780 to 960 nm) absorption and emission coexist in few-layer MoS_2.[25] The PL spectrum in Figure 1e, consisting of one major peak at 670 nm and one minor peak at 610 nm, further confirms the band gap of our few-layer MoS_2. The two feature peaks indicate the direct band transitions of excitons between the maximum of the split valence bands and the minimum of the conduction band at the K point of the Brillouin zone.[25] The splitting of valence bands is due to the combined effect of interlayer coupling and spin−orbit coupling.[23,25] The 610 nm emission can be observed only in few-layer MoS_2, while 670 nm emission is monolayer-related luminescence, which is decreased with the thickness of the few-layer MoS_2. The optical absorption spectrum of three-layer MoS_2 in Figure 1f reveals that the absorption coefficient of few-layer MoS_2 is up to 7.5×10^5 cm^{-1} in the visible wavelength region, indicating that three-layer MoS_2 can absorb ∼10% of incident light.[33] In addition, the two optical absorption peaks also match the direct excitonic transition peaks of MoS_2 at around 610 and 670 nm observed in the PL spectrum, as shown in Figure 1e.

Figure 2a−b show the schematic and the optical microscopic top-view image of the MoS_2 PDs, respectively. In order to boost the photosensitivity of the few-layer MoS_2, the devices were fabricated in MSM geometry with Schottky contacts to MoS_2 to effectively lower the dark current. Accordingly, 100 nm thick Au layers as Schottky contacts were deposited on few-layer MoS_2 using electron beam deposition. Figure 2c presents the photocurrent as a function of time under 532 nm laser illumination (light intensity $I_{light} = 2.0 \times 10^4$ W/m^2) under different bias conditions. Under illumination, the current rises to a high value (ON state) and then returns to a low value when the light is off (OFF state). As the applied bias is increased to the "flat-band" voltage, *i.e.*, ∼10 V, the photocurrent becomes saturated, indicating the formation of a full depletion of the few-layer MoS_2 between the two electrodes. The transition between ON and OFF states reveals the response/recovery speed of the MoS_2 PDs. The results are shown in Figure 2d, from which the rise time (from 10% to 90% of the maximum photocurrent as switching light from OFF to ON) and the fall time (from 90% to 10% of the maximum photocurrent as switching light from ON to OFF) of MoS_2 MSM PDs can be estimated to be 70 and 110 μs, respectively. The photoresponse times of MoS_2 MSM PDs measured in this study are 3 orders of magnitude shorter than those reported previously (∼50 ms).[26] The difference of the response speed between the work done in ref 26 and our work could be explained from three aspects. First of all, the contact electrode to MoS_2 in our work is pure Au with a high work function of 5.47 eV.[34] The two back-to-back Schottky contacts to MoS_2 formed by the high-work-function metal lead to low dark current (due to the presence of two back-to-back Schottky barriers) and fast photoresponse speed (due to fast carrier sweeping in the depletion regions under the electric fields of the reverse bias Schottky barrier).[35] We further estimated the electric fields of the reverse bias Schottky barrier under 5 V bias to be more than 6×10^5 V/m by $E = V/L$, where E is the electrical field, V is the applied voltage, and L is the contact spacing. As the bias voltage increases, the electric fields of the reverse bias Schottky barrier will increase. Second, we employed the MSM structure with the "interdigital" electrode pattern, which can facilitate the efficient collection of photocarriers and contribute to faster response speed. Third, the difference between two works (ref 26 and ours) may not merely come from the device, but the improvement of the measurement system. The time resolution of our measurement system is 10 μs, which is apparently higher than that of ref 26 (∼tens of milliseconds). Moreover, we do note that the photoresponse times could be further improved *via* increasing the Schottky barrier height between contact metal and MoS_2 as well as reducing surface defects and metal contact spacing.[29,36,37]

To demonstrate the feasibility of few-layer MoS_2 PDs in practical uses, the following investigations were performed, including (i) spectral responsivity, (ii) light intensity-dependent photocurrent, and (iii) light modulation frequency-dependent photogain measurements, as shown in Figure 3a−c, respectively. In Figure 3a, spectral responsivity and photogain of the MoS_2 MSM PDs were measured under a bias of 10 V. Within the visible wavelength region the responsivity is up to 0.57 A/W at 532 nm, where the cutoff wavelength of ∼660 nm agrees with the direct band gap of the MoS_2 films (∼1.9 eV).[24,25] Note that ultrahigh responsivity up to 0.57 A/W obtained here is 3 orders of

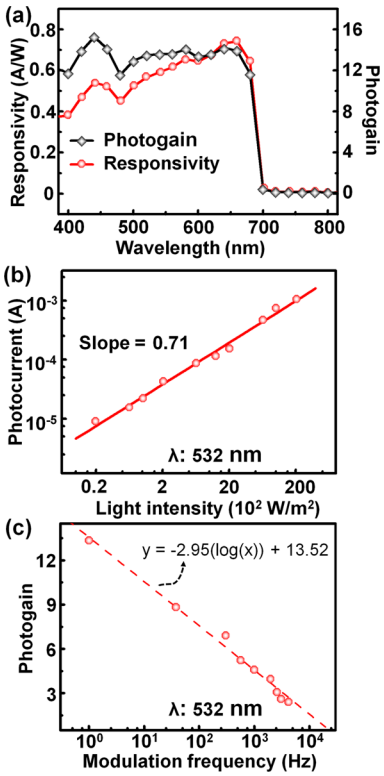

Figure 3. (a) Photogain and responsivity as a function of wavelength measured under a bias of 10 V. (b) Light intensity-dependent photocurrent of the MoS_2 PDs at 10 V. (c) Frequency dependence of the photogain measured under a bias of 10 V and 532 nm laser illumination (I_{light} = 2.0 × 10^4 W/m^2).

magnitude higher than ~7.5 × 10^{-3} A/W obtained by the MoS_2 phototransistors.[26] Measured photoresponsivity from the MoS_2 MSM PDs is also much higher than that obtained from the graphene phototransistors (1 × 10^{-3} A/W).[13,14] The photogain of the MoS_2 PD with 8 μm long contact spacing can be further estimated to be up to 13.3 by $R = I_p/P = \eta_{ext}Gq/h\nu$, where R is the responsivity, I_p is the total generated photocurrent of the whole device, P is the total incident light power over the device, η_{ext} is the external quantum efficiency (assumed to be 10% due to ~10% of the optical absorption of MoS_2 over the visible region), G is the photogain, q is the electronic charge, h is Planck's constant, and ν is the frequency of the incident wavelength.[38] The photogain greater than unity is first observed in the PDs based on 2D nanomaterials, leading to the ultrahigh responsivity. It should be noted that most conventional Schottky MSM PDs show no photogain.[35] The photogain greater than unity in the MSM Schottky PDs has been observed previously. The photogain in MSM PDs is attributed to the injection of photocarriers by tunneling from the contact into the semiconductor. The photocarrier injection is caused by carriers trapped at surface defects in the vicinity of the contact.[39−41] The ultralarge surface-to-volume ratio in 2D nanomaterials implies that significant surface states would be produced in the semiconductor−metal interface. Accordingly, under illumination, the photocarriers trapped by surface states at the semiconductor−metal interface lead to the reduction of the Schottky barrier height and the production of photogain of MoS_2 MSM PDs greater than unity.[38−41]

Moreover, the noise equivalent power (NEP) is an important parameter of a PD that is frequently quoted, *i.e.*, the optical signal power required to generate a photocurrent signal (I_{ph}) that is equal to the total noise current (I_n) in the PD at a given wavelength and within a bandwidth of 1 Hz.[42,43] The NEP represents the required optical power to achieve a signal-to-noise ratio (SNR) of 1 with a bandwidth of 1 Hz. The detectivity (D^*), the reciprocal of NEP, is a figure of merit used to characterize the performance of a photodetector. Under a 10 V bias, the calculated NEP of the MoS_2 MSM PDs in this study is 1.1 × 10^{-10} W/cm Hz$^{1/2}$ by NEP = $P/f^{1/2} = (2eJ_d)^{1/2}/R$, where P is incident optical power, f is frequency bandwidth of the photodetector, R is responsivity, e is electronic charge, and J_d is dark current density, leading to a D^* of ~10^{10} cm Hz$^{1/2}$/W.[42,43] To compare with commercially available AlGaN-based PDs (2.65 × 10^{10} cm Hz$^{1/2}$/W) and Si-based PDs (~10^{12} cm Hz$^{1/2}$/W) reported previously,[44,45] the detectivity of few-layer MoS_2 MSM PDs should be further improved *via* reducing the dark current and increasing the responsivity.

To quantitatively analyze the relationship of the photoresponse to the light intensity, the photocurrent was measured under a bias of 10 V with I_{light}, as shown Figure 3b. Measurements were performed from low to high light intensity to prevent artifacts caused by persistence or temperature transients. The photocurrent (I_{ph}) *versus* I_{light} is fitted by a power-law relationship ($I_{ph} \approx (I_{light})^n$) with $n = 0.71$, by which a near-linear relationship can be obtained. The generation rate of photocarriers is proportional to the amount of photon absorption, implying that the defects in the few-layer MoS_2 contribute little to the photocurrent.[46]

The dynamics of the photogenerated carriers can be further manifested based on the high-frequency measurement of the MoS_2 PDs. The measurement was carried out under a bias of 10 V with a mechanical chopper to modulate the frequency of light sources.[9] As shown in Figure 3c, the photogain gradually reduces with the modulation frequency due to the limitation of response rates. One can see that even in the sub-millisecond domain the photogain values are still larger than unity. We note that the defects in the MoS_2 limit the performance of MoS_2 PDs; carrier mobility, photoresponse time, and responsivity can be further improved *via* reducing the defects in the MoS_2 layers. We envision that once the defect can be eliminated significantly, the performance of superior crystalline MSM PDs is boosted further with an appropriate device design.

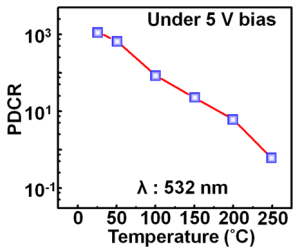

Figure 4. PDCR of MoS_2 PDs as a function of temperature measured under a bias of 5 V and 532 nm laser illumination ($I_{light} = 2.0 \times 10^4$ W/m^2).

To demonstrate photodetection applications under harsh conditions, the thermal stability of the MoS_2 PDs is evaluated by measuring the photocurrent/dark current ratio (PDCR = $(I_{ph} - I_d)/I_d$, where I_{ph} is the photocurrent under illumination and I_d is the dark current) from room temperature to 250 °C.[28,50] The PDCR curve in Figure 4 shows that the few-layer MoS_2 PDs are capable of photodetection even at 200 °C, mainly due to small levels of current leakage and high thermal stability of MoS_2 at high temperatures. A further increase in temperature lowers the PDCR of MoS_2 PDs. When the temperature increases to 250 °C, the PDCR value decreases to unity, indicating that the MoS_2 PDs cannot work properly. The noticeable deterioration in PD performance may be due to the oxidization of few-layer MoS_2 and the generation of the thermal carriers, which cannot be eliminated at high temperatures.[51] It should be noted that the oxidation of MoS_2 to MoO_3 in a dry O_2 environment could occur at 375 K.[52] Moreover, Mikheev *et al.* have also reported that the degradation of the nanographite film PD sensitivity is caused by the oxidation of the nanographite at high temperature.[53] Therefore, we envision that further improvements including the passivation layers for preventing oxidation, reducing surface defects, and reinforcing the Au/MoS_2 interface might be able to extend the working temperatures of MoS_2 PDs.[28,54]

CONCLUSION

In summary, for the first time, 2D nanomaterials using few-layer MoS_2 as MSM PDs with broadband high responsivity/photogain and fast photoresponse for applications in harsh environments are demonstrated. The broadband absorption feature of few-layer MoS_2 was not achievable previously for harsh environment use since all materials for harsh environments are wide-band-gap semiconductors. At 10 V bias, the photogain of up to 13.3 leads to ultrahigh responsivity and detectivity of MoS_2 up to 0.57 A/W and $\sim 10^{10}$ cm Hz$^{1/2}$/W, respectively, which was not obtainable in pristine graphene and MoS_2-based PDs before. The MoS_2 MSM PDs exhibit a very fast and stable photoresponse, *i.e.*, ~70 μs of rise time and ~110 μs of fall time. Although the thickness of few-layer MoS_2 is only ~1.9 nm, the optical absorption of MoS_2 is as high as ~10% over the visible region. Furthermore, few-layer MoS_2 shows an excellent sensitivity factor (PDCR) that is up to ~10 even at 200 °C. Few-layer MoS_2, a new class of 2D nanomaterials with broadband high photogain and fast optical switching, holds promise for the next-generation optical devices in harsh conditions.

METHODS

For the preparation of few-layer MoS_2, 0.25 g of $(NH_4)_2MoS_4$ (Alfa Aesar, purity of 99.99%) was added to 20 mL of DMF to form a 1.25 wt % solution. It was sonicated for 20 min to achieve a homogeneous $(NH_4)_2MoS_4$ solution. The sapphire substrates were first cleaned with a piranha solution (H_2SO_4/H_2O_2, 7:3) to remove the surface contaminants. The cleaned substrates were immersed into the $(NH_4)_2MoS_4$ solution, followed by slow pulling-up (0.5 mm/s). After that, the substrates were baked on a hot plate at 120 °C for 30 min until the majority of solvent molecules were evaporated. The substrate was then placed on the edge of a quartz tube with a flow of H_2 (20 sccm) and Ar (80 sccm). When the temperature in the center of the furnace reached 500 °C, the substrate was moved to the center of the furnace. Sixty minutes later, the sample was cooled to room temperature under H_2/Ar ambient by putting the sample back to the tube edge. The sample was moved to the furnace center again for the second postannealing when the center of the furnace reached 1000 °C in an Ar^+ sulfur environment at 500 Torr. After the process of growing MoS_2 layers on sapphire, we transferred the MoS_2 layers onto freshly cleaned SiO_2/Si substrates for fabricating MSM PDs.

The MSM PDs were defined using photolithography with active areas of $500 \times 158\ \mu m^2$, and 8 μm wide, 150 μm long, and 100 nm thick interdigitated Au electrodes with 8 μm wide spacing to serve as Schottky contacts on MoS_2/SiO_2/Si substrates were utilized for the MSM PDs. The MoS_2 MSM PDs were measured under 532 nm laser (beam diameter is ~1 mm) illumination in air.

After the fabrication process of MoS_2 MSM Schottky PDs, surface morphology and thickness of the atomically thin MoS_2 were revealed by atomic force microscopy (Veeco Dimension-Icon system). Raman and PL spectra were obtained by confocal Raman microscopic systems (NT-MDT) with a 473 nm laser (spot size of laser is ~0.5 μm in diameter). The Si peak at 520 cm^{-1} was used for calibration in the experiments. Field-emission transmission electron microscopy (JEOL JEM-2100F, operated at 200 kV with a point-to-point resolution of 0.19 nm) was used to investigate the microstructures. The samples for HRTEM were prepared using a lacy-carbon Cu grid to scratch the surface of MoS_2 samples. The absorbance spectra were measured with a JASCO V-670 UV−visible spectrometer in the spectral range from 380 to 800 nm. The Keithley 4200-SCS semiconductor characterization system and the EQE-R3011 spectral response system (Enli Technology Co., Ltd.) were used to measure $I-V$ characteristics and responsivity of the few-layer MoS_2 PDs.

Conflict of Interest: The authors declare no competing financial interest.

Acknowledgment. This work was supported by National Science Council of Taiwan (99-2622-E-002-019-CC3, 99-2112-M-002-024-MY3, and 99-2120-M-007-011) and National Taiwan University (10R70823). L.-J.L. also acknowledges the support from Academia Sinica (IAMS and Nano program).

REFERENCES AND NOTES

1. Mas-Balleste, R.; Gomez-Navarro, C.; Gomez-Herrero, J.; Zamora, F. 2D Materials: To Graphene and Beyond. *Nanoscale* **2011**, *3*, 20–30.
2. Novoselov, K. S.; Jiang, D.; Schedin, F.; Booth, T. J.; Khotkevich, V. V.; Morozov, S. V.; Geim, A. K. Two-Dimensional Atomic Crystals. *Proc. Natl. Acad. Sci. U.S.A.* **2005**, *102*, 10451–10453.
3. Radisavljevic, B.; Whitwick, M. B.; Kis, K. Integrated Circuits and Logic Operations Based on Single-Layer MoS_2. *ACS Nano* **2011**, *5*, 9934–9938.
4. Osada, M.; Sasaki, T. Two-Dimensional Dielectric Nanosheets: Novel Nanoelectronics from Nanocrystal Building Blocks. *Adv. Mater.* **2012**, *24*, 210–228.
5. Ko, H.; Takei, K.; Kapadia, R.; Chuang, S.; Fang, H.; Leu, P. W.; Ganapathi, K.; Plis, E.; Kim, H. S.; Chen, S. Y. Ultrathin Compound Semiconductor on Insulator Layers for High-Performance Nanoscale Transistors. *Nature* **2010**, *468*, 286–289.
6. Geim, A. K.; Novoselov, K. S. The Rise of Graphene. *Nat. Mater.* **2007**, *6*, 183–191.
7. Howard, R. S.; Dennis, G. H. Island Size Effects in Nanoparticle-Enhanced Photodetectors. *Appl. Phys. Lett.* **1998**, *73*, 3815–3818.
8. Chen, C. Y.; Retamal, J. R. D.; Lien, D. H.; Chen, M. W.; Wu, I. W.; Ding, Y.; Chueh, Y. L.; Wu, C. I.; He, J. H. Probing Surface Band Bending of Surface-Engineered Metal Oxide Nanowires. *ACS Nano* **2012**, *6*, 9366–9372.
9. Soci, C.; Zhang, A.; Xiang, B.; Dayeh, S. A.; Aplin, D. P. R.; Park, J.; Bao, X. Y.; Lo, Y. H.; Wang, D. ZnO Nanowire UV Photodetectors with High Internal Gain. *Nano Lett.* **2007**, *7*, 1003–1009.
10. Chen, C. Y.; Chen, M. W.; Ke, J. J.; Lin, C. A.; Retamal, J. R. D.; He, J. H. Surface Effects on Optical and Electrical Properties of ZnO Nanostructures. *Pure Appl. Chem.* **2010**, *82*, 2055–2073.
11. Gao, P.; Wang, Z. Z.; Liu, K. H.; Xu, Z.; Wang, W. L.; Bai, X. D.; Wang, E. G. Photoconducting Response on Bending of Individual ZnO Nanowires. *J. Mater. Chem.* **2009**, *19*, 1002–1005.
12. Chen, M. W.; Chen, C. Y.; Lien, D. H.; Ding, Y.; He, J. H. Photoconductive Enhancement of Single ZnO Nanowire through Localized Schottky Effects. *Opt. Express* **2010**, *18*, 14836–14841.
13. Xia, F.; Mueller, T.; Golizadeh-Mojarad, R.; Freitag, M.; Lin, Y. M.; Tsang, J.; Perebeinos, V.; Avouris, P. Photocurrent Imaging and Efficient Photon Detection in a Graphene Transistor. *Nano Lett.* **2009**, *9*, 1039–1044.
14. Xia, F.; Mueller, T.; Lin, Y. M.; Valdes-Garcia, A.; Avouris, P. Ultrafast Graphene Photodetector. *Nat. Nanotechnol.* **2009**, *4*, 839–843.
15. Mueller, T.; Xia, F.; Avouris, P. Graphene Photodetectors for High-Speed Optical Communications. *Nat. Photon.* **2010**, *4*, 297–301.
16. Bonaccorso, F.; Sun, Z.; Ferrari, A. C. Graphene Photonics and Optoelectronics. *Nat. Photon.* **2010**, *4*, 611–621.
17. Konstantatos, G.; Badioli, M.; Gaudreau, L.; Osmond, J.; Bernechea, M.; de Arquer, F. P. G.; Gatti, F.; Koppens, F. H. L. Hybrid Graphene–Quantum Dot Phototransistors with Ultrahigh Gain. *Nat. Nanotechnol.* **2012**, *7*, 363–368.
18. Echtermeyer, T. J.; Britnell, L.; Jasnos, P. K.; Lombardo, A.; Gorbachev, R. V.; Grigorenko, A. N.; Geim, A. K.; Ferrari, A. C.; Novoselov, K. S. Strong Plasmonic Enhancement of Photovoltage in Graphene. *Nat. Commun.* **2011**, *2*, 458.
19. Liu, Y.; Cheng, R.; Liao, L.; Zhou, H.; Bai, J.; Liu, G.; Liu, L.; Huang, Y.; Duan, X. Plasmon Resonance Enhanced Multicolour Photodetection by Graphene. *Nat. Commun.* **2011**, *2*, 579–585.
20. Furchi, M.; Urich, A.; Pospischil, A.; Lilley, G.; Unterrainer, K.; Detz, H.; Klang, P.; Andrews, A. M.; Schrenk, W.; Strasser, G.; Mueller, T. Microcavity-Integrated Graphene Photodetector. *Nano Lett.* **2012**, *12*, 2773–2777.
21. Radisavljevic, B.; Radenovic, A.; Brivio, J.; Giacometti, V.; Kis, A. Single-Layer MoS_2 Transistors. *Nat. Nanotechnol.* **2011**, *6*, 147–150.
22. Zhang, Y.; Ye, J.; Matcuhashi, Y.; Iwasa, Y. Ambipolar MoS_2 Thin Flake Transistors. *Nano Lett.* **2012**, *12*, 1136–1140.
23. Liu, K. K.; Zhang, W.; Lee, Y. H.; Lin, Y. C.; Chang, M. T.; Su, C. Y.; Chang, C. S.; Li, H.; Shi, Y.; Zhang, H. Growth of Large-Area and Highly Crystalline MoS_2 Thin Layers on Insulating Substrates. *Nano Lett.* **2012**, *12*, 1538–1544.
24. Eda, G.; Yamaguchi, H.; Voiry, D.; Fujita, T.; Chen, M.; Chhowalla, M. Photoluminescence from Chemically Exfoliated MoS_2. *Nano Lett.* **2011**, *11*, 5111–5116.
25. Mak, K. F.; Lee, C.; Hone, J.; Shan, J.; Heinz, T. F. Atomically Thin MoS_2: A New Direct-Gap Semiconductor. *Phys. Rev. Lett.* **2010**, *105*, 136805.
26. Yin, Z.; Li, H.; Li, H.; Jiang, L.; Shi, Y.; Sun, Y.; Lu, G.; Zhang, Q.; Chen, X.; Zhang, H. Single-Layer MoS_2 Phototransistors. *ACS Nano* **2012**, *6*, 74–80.
27. Casady, J. B.; Johnson, R. W. Status of Silicon Carbide (SiC) as a Wide-Bandgap Semiconductor for High-Temperature Applications: A Review. *Solid-State Electron.* **1996**, *39*, 1409–1422.
28. Lien, W. C.; Tsai, D. S.; Chiu, S. H.; Senesky, D. G.; Maboudian, R.; Pisano, A. P.; He, J. H. Low-Temperature, Ion Beam Assisted SiC Thin Films with Antireflective ZnO Nanorod Arrays for High-Temperature Photodetection. *IEEE Electron Device Lett.* **2011**, *32*, 1564–1566.
29. Tsai, D. S.; Lin, C. A.; Lien, W. C.; Chang, H. C.; Wang, Y. L.; He, J. H. Ultra-High-Responsivity Broadband Detection of Si Metal–Semiconductor–Metal Schottky Photodetectors Improved by ZnO Nanorod Arrays. *ACS Nano* **2011**, *5*, 7748–7753.
30. Brown, D. M.; Downey, E. T.; Ghezzo, M.; Kretchmer, J. W.; Saia, R. J.; Liu, Y. S.; Edmond, J. A.; Gati, G.; Pimbley, J. M.; Schneider, W. E. Silicon Carbide UV Photodiodes. *IEEE Trans. Electron Devices* **1993**, *40*, 325–333.
31. Lee, Y. H.; Zhang, X. Q.; Zhang, W.; Chang, M. T.; Lin, C. T.; Chang, K. D.; Yu, Y. C.; Wang, J. T.; Chang, C. S.; Li, L. J. Synthesis of Large-Area MoS_2 Atomic Layers with Chemical Vapor Deposition. *Adv. Mater.* **2012**, *24*, 2320–2325.
32. Su, C. Y.; Lu, A. Y.; Wu, C. Y.; Li, Y. T.; Liu, K. K.; Zhang, W.; Lin, S. Y.; Juang, Z. Y.; Zhong, Y. L.; Chen, F. R. Direct Formation of Wafer Scale Graphene Thin Layers on Insulating Substrates by Chemical Vapor Deposition. *Nano Lett.* **2011**, *11*, 3612–3616.
33. Gourmelon, E.; Lignier, O.; Hadouda, H.; Couturier, G.; Bernède, J. C.; Tedd, J.; Pouzet, J.; Salardenne, J. MS_2 (M = W, Mo) Photosensitive Thin Films for Solar Cells. *Sol. Energy Mater. Sol. Cells* **1997**, *46*, 115–121.
34. Dhara, S.; Giri, P. K. On the Origin of Enhanced Photoconduction and Photoluminescence from Au and Ti Nanoparticles Decorated Aligned ZnO Nanowire Heterostructures. *J. Appl. Phys.* **2011**, *110*, 124317.
35. Razeghi, M.; Rogalski, A. Semiconductor Ultraviolet Detectors. *J. Appl. Phys.* **1996**, *79*, 7433–7473.
36. Chou, S. Y.; Liu, M. Y. Nanoscale Tera-Hertz Metal–Semiconductor–Metal Photodetectors. *IEEE J. Quantum Electron.* **1992**, *28*, 2358–2368.
37. Li, M.; Anderson, W. A. Si-Based Metal–Semiconductor–Metal Photodetectors with Various Design Modifications. *Solid-State Electron.* **2007**, *51*, 94–101.
38. Yang, Q.; Guo, X.; Wang, W.; Zhang, Y.; Xu, S.; Lien, D. H.; Wang, Z. L. Enhancing Sensitivity of a Single ZnO Micro-/Nanowire Photodetector by Piezo-Phototronic Effect. *ACS Nano* **2010**, *10*, 6285–6291.
39. Mehta, R. R.; Sharma, B. S. Photoconductive Gain Greater than Unity in CdSe Films with Schottky Barriers at Contacts. *J. Appl. Phys.* **1973**, *44*, 325–328.
40. Katz, O.; Garber, V.; Meyler, B.; Bahir, G.; Salzman, J. Gain Mechanism in GaN Schottky Ultraviolet Detectors. *Appl. Phys. Lett.* **2001**, *79*, 1417–1419.
41. Klingenstein, M.; Kuhl, J.; Rosenzweig, J.; Moglestue, C.; Hülsmann, A.; Schneider, J.; Köhler, K. Photocurrent Gain Mechanisms in Metal-Semiconductor-Metal Photodetectors. *Solid-State Electron.* **1994**, *37*, 333–340.
42. Kasap, S. O. *Optoelectronics and Photonics*; Prentice Hall International: Englewood Cliffs, NJ, 2001.

43. Gong, X.; Tong, M.; Xia, Y.; Cai, W.; Moon, J. S.; Cao, Y.; Yu, G.; Shieh, C. L.; Nilsson, B.; Heeger, A. J. High-Detectivity Polymer Photodetectors with Spectral Response from 300 to 1450 nm. *Science* **2009**, *325*, 1665–1667.
44. Lee, K. H.; Chang, P. C.; Chang, S. J.; Wang, Y. C.; Yu, C. L.; Wu, S. L. Characterization of AlGaN/GaN MetalSemiconductor-Metal Photodetectors with a Low-Temperature AlGaN Interlayer. *IEEE Sens. J.* **2009**, *9*, 723–727.
45. Wegrzecka, I.; Wegrzecki, M.; Grynglas, M.; Bar, J.; Uszynski, A.; Grodecki, R.; Grabiec, P.; Krzeminski, S.; Budzynski, T. Design and Properties of Silicon Avalanche Photodiodes. *Opto-Electronics Rev.* **2004**, *12*, 95–104.
46. Li, C.; Bando, Y.; Liao, M.; Koide, Y.; Golberg, D. Visible-Blind Deep-Ultraviolet Schottky Photodetector with a Photocurrent Gain Based on Individual Zn_2GeO_4 Nanowire. *Appl. Phys. Lett.* **2010**, *97*, 161102.
47. Soci, C.; Zhang, A.; Bao, X. Y.; Kim, H.; Lo, Y.; Wang, D. Nanowire Photodetectors. *J. Nanosci. Nanotechnol.* **2010**, *10*, 1–20.
48. Wang, R.; Ruzicka, B. A.; Kumar, N.; Bellus, M. Z.; Chiu, H. Y.; Y., H.; Zhao, H. Ultrafast and Spatially Resolved Studies of Charge Carriers in Atomically Thin Molybdenum Disulfide. *Phys. Rev. B* **2012**, *86*, 045406.
49. Korn, T.; Heydrich, S.; Hirmer, M.; Schmutzler, J.; Schuller, C. Low-Temperature Photocarrier Dynamics in Monolayer MoS_2. *Appl. Phys. Lett.* **2011**, *99*, 102109.
50. Tsai, D. S.; Kang, C. F.; Wang, H. H.; Lin, C. A.; Ke, J. J.; Chu, Y. H.; He, J. H. n-ZnO/$LaAlO_3$/p-Si Heterojunction for Visible-Blind UV Detection. *Opt. Lett.* **2012**, *37*, 1112–1114.
51. Vijayakumar, A.; Todi, R. M.; Sundaram, K. B. Amorphous-SiCBN-Based Metal−Semiconductor−Metal Photodetector for High-Temperature Applications. *IEEE Electron Device Lett.* **2007**, *28*, 713–715.
52. Windom, B. C.; Sawyer, W. G.; Hahn, D. A. A Raman Spectroscopic Study of MoS_2 and MoO_3: Applications to Tribological Systems. *Tribol. Lett.* **2011**, *42*, 301–310.
53. Mikheev, G. M.; Zonov, R. G.; Obraztsov, A. N.; Svirko, Y. P. Sensitivity of Fast-Response Nanographite Photodetector at High Temperature. *Proc. SPIE* **2009**, *7356*, 1–8.
54. Vescan, A.; Daumiller, I.; Gluche, P.; Ebert, W.; Kohn, E. High Temperature, High Voltage Operation of Diamond Schottky Diode. *Diam. Relat. Mater.* **1998**, *7*, 581–584.